Journal of Biomechanics 48 (2015) 1662–1670

Contents lists available at ScienceDirect

Journal of Biomechanics

journal homepage: www.elsevier.com/locate/jbiomech
www.JBiomech.com

Transition from fetal to neonatal circulation: Modeling the effect of umbilical cord clamping

Mehmet B. Yigit [a], William J. Kowalski [b], David J.R. Hutchon [c], Kerem Pekkan [a,d,*]

[a] Department of Biomedical Engineering, Carnegie Mellon University, Pittsburgh, PA, USA
[b] Cardiovascular Innovation Institute, University of Louisville, Louisville, KY, USA
[c] Memorial Hospital, Darlington DL3 6HX, UK
[d] Department of Mechanical Engineering, Koç University, Rumelifeneri Yolu, Sariyer, Istanbul, Turkey

ARTICLE INFO

Article history:
Accepted 17 February 2015

Keywords:
Fetal hemodynamics
Fetal-to-neonatal transition
Umbilical cord clamping
Delayed umbilical cord clamping
Lumped parameter model
Cardiovascular dynamics

ABSTRACT

Hemodynamics of the fetal to neonatal transition are orchestrated through complex physiological changes and results in cardiovascular adaptation to the adult biventricular circulation. Clinical practice during this critical period can influence vital organ physiology for normal newborns, premature babies and congenital heart defect patients. Particularly, the timing of the cord clamping procedure, immediate (ICC) *vs.* delayed cord clamping (DCC), is hypothesized to be an important factor for the *transitory fetal hemodynamics*. The clinical need for a quantitative understanding of this physiology motivated the development of a lumped parameter model (LPM) of the fetal cardio-respiratory system covering the late-gestation to neonatal period. The LPM was validated with *in vivo* clinical data and then used to predict the effects of cord clamping procedures on hemodynamics and vital gases. Clinical time-dependent resistance functions to simulate the vascular changes were introduced. For DCC, placental transfusion (31.3 ml) increased neonatal blood volume by 11.7%. This increased blood volume is reflected in an increase in preload pressures by ~20% compared to ICC, which in turn increased the cardiac output (CO) by 20% (CO_{ICC}=993 ml/min; CO_{DCC}=1197 ml/min). Our model accurately predicted dynamic flow patterns *in vivo*. DCC was shown to maintain oxygenation if the onset of pulmonary respiration was delayed or impaired. On the other hand, a significant 25% decrease in oxygen saturations was observed when applying ICC under the same physiological conditions. We conclude that DCC has a significant impact on newborn hemodynamics, mainly because of the improved blood volume and the sustained placental respiration.

1. Introduction

Circulatory physiology of the newborn goes through complex transitions in order to shift the respiratory function from the placenta to the lungs, characterized by the closure of fetal shunts, expansion of the lungs, and removal of placental circulation (Friedman and Fahey, 1993; Rudolph, 1970). In order to speed up and manage the fetal-to-neonatal transition, immediate cord clamping (ICC) has been adopted as a standard clinical practice. However, this practice has been challenged, as recent findings demonstrated that delaying the cord clamping (DCC) for at least 30–60 s can be beneficial for the neonate, especially for the preterm due to the transfusion of placental resources (ACOG's Committee on Obstetric Practice, 2012; Hutchon, 2013; Raju, 2013), however it is possible to increase the net effect of transfusion by prolonging the timing of DCC considering that umbilical flow persists as long as 5 to 10 min after birth (Boere et al., 2015; Usher et al., 1963). Recent *in vivo* studies in preterm lambs indicated that DCC improves cardiovascular function through improved hemodynamic stability and increased cardiac output (CO) during the first 30 min after cord clamping (Bhatt et al., 2013). In preterm infants, both superior vena cava return and right ventricle output (RVO) were higher for the DCC group compared to the ICC over the critical first 2 days of life (Sommers et al., 2012). These observations strengthen the view that ICC can lead to reduced cardiovascular function due to hypovolemia and irregular neonatal hemodynamics (Hutchon, 2013).

ICC is also associated with lower peripheral oxygen saturation at birth (Smit et al., 2014). Prediction of fundamental vasoactive gases in relation to the cord clamping procedures is essential as placental flow is associated with the expansion of the lungs and remodeling of fetal shunts as it carries important vasoactive agents such as oxygen and prostaglandins PGE_2 (Coceani and Olley, 1973; Friedman and Fahey, 1993; Hutchon, 2013). Therefore, ICC has the likelihood of altering the fetal transition through multiple pathways where the hemodynamic and respiratory components can be

* Correspondence to: Mechanical Engineering Department, Koç University, Rumelifeneri Yolu, Sariyer, Istanbul, Turkey. Tel.: +1 412 623 9378.
E-mail address: kpekkan@ku.edu.tr (K. Pekkan).

http://dx.doi.org/10.1016/j.jbiomech.2015.02.040
0021-9290/

dissected. Models and quantitative information of the early neonatal circulation and the effects of cord clamping are particularly required for the investigation of new management strategies during neonatal resuscitation (Niermeyer and Velaphi, 2013) and devices (Hutchon, 2013).

Our aims in this study are to 1) construct a physiologically accurate and detailed lumped parameter model (LPM) of the transition from fetal-to-neonatal circulation at birth and 2) investigate and compare the two cord clamping scenarios, namely DCC and ICC, based on their relative impacts on hemodynamics and respiration in the transitioning circulation of a term infant. In our simulations, we adopted a prolonged DCC case in order to observe the full effect of placental transfusion on the newborn, in which the clamp is applied after the umbilical flow completely ceases due to physiological constriction of umbilical arteries. ICC is simulated as standard in which clamp is applied at the beginning of transition.

To our knowledge, a *system-level* hemodynamic investigation of the *continuous* transition from fetal-to-neonatal circulation in the human has not been undertaken except for a simplified representation without gas exchange, whilst isolated lumped parameter studies of the fetal circulation at late gestation are available in the literature (Huikeshoven et al., 1985; Pennati et al., 1997; Pennati and Fumero, 2000; Sa-Couto et al., 2010). We believe that the present model would be important for neonatologists in understanding the fetal transition in detail and to improve clinical interventions with the transitioning fetal circulation. In the following sections, we use the abbreviations defined in Fig. 1 to refer to the LPM organ compartments and vessels. This format was chosen in order to avoid excessive in-text explanations of acronyms. A list of abbreviations is also given in Table 1.

2. Methods

2.1. Hemodynamic model

Using our neonatal and pediatric circulatory LPM framework (Pekkan et al., 2005; Peskin and Tu, 1986; Sundareswaran et al., 2008), we constructed a representative fetal circuit (Fig. 1) inspired from an earlier design by Pennati et al. (Pennati et al., 1997). Compliance (C) chambers were used to model major

Table 1
List of abbreviations.

Table of abbreviations			
ICC	Immediate cord clamping	R	Resistance
DCC	Delayed cord clamping	C	Compliance
LPM	Lumped parameter model	τ	Transition time
CO	Cardiac output	r	Ventilation–perfusion ratio
CCO	Combined cardiac output	EF	Ejection fraction of the ventricle
SO_2	Oxygen saturation	LVO	Left ventricular output
$[O_2]$	Oxygen concentration	RVO	Right ventricular output
PO_2	Partial pressure of oxygen	LV	Left ventricle
Q	Flow rate	RV	Right ventricle
P	Pressure	DA	Ductus arteriosus
V	Volume		

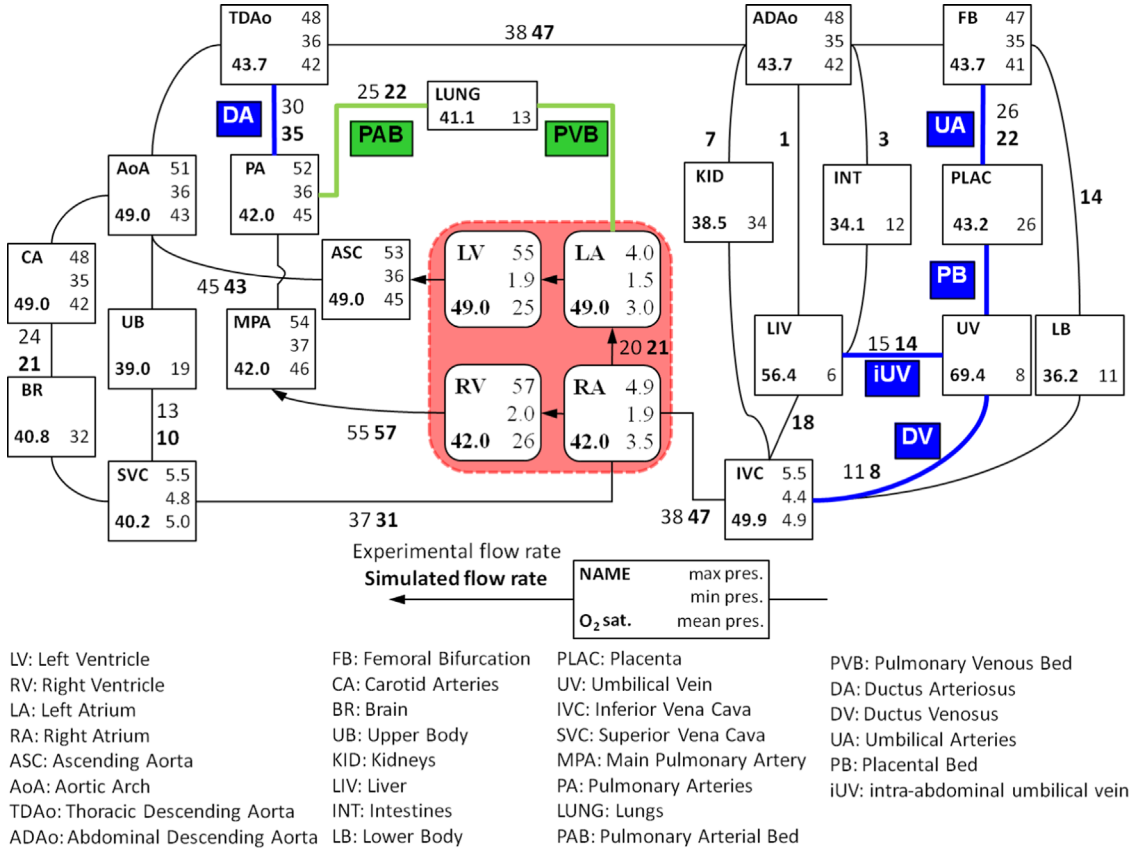

Fig. 1. Network schematics of the transitionary fetal cardiovascular circuit. Connecting lines represent arterial, capillary and venous resistance elements, and compartments correspond to compliance chambers. Arrows describe the direction of trans-valvular flow. Cycle-averaged flow rate distributions as a percentage of combined cardiac output (%CCO) is labeled on the connecting vessels (CCO=1.5 l/min), simulated flow rates are displayed in bold, experimental *in vivo* flow rates are selected values that were obtained from the literature (Kiserud et al., 2006; Mielke and Benda, 2001; Molina et al., 2008; Rasanen et al., 1996; Rudolph, 2009). Minimum–maximum-mean pressures (mmHg), and oxygen saturations (SO_2%) as well as the names of the compartments are displayed in boxes. All values correspond to the fetal circulation just before birth at the late-gestation period. *Blue* colored vessels represent the connections that close and *green* color represents connections that open during the fetal-to-neonatal transition. (For interpretation of the references to color in this figure legend, the reader is referred to the web version of this article.)

vascular compartments, which were connected with linear resistance (R) components that represent the viscous drag. Each R–C compartment model is governed by a differential equation:

$$\frac{d(CP)_i}{dt} = \sum_{j=1}^{N} \frac{P_j - P_i}{R_{ji}} \tag{1}$$

where P is the pressure in the compliance compartments labeled by their subscripts i and j, N is the number of lumped compliance compartments. R_{ji} has a finite value if it allows flow from compartment j to compartment i, otherwise it is infinite. Subscripts i and j label the compliance compartments and their associated parameters (P, V, $[O_2]$), where V is volume and $[O_2]$ is oxygen concentration, and double subscripts ij and ji label resistive elements located between compartments i and j. The order of subscripts indicates the positive direction of their associated parameters (*e.g.* $Q_{ij} > 0$ means that the flow is from i to j).

A classical time-varying elastance function ($E(t)$) (Suga et al., 1973) was used for the ventricles and atria as the driving function for the pulsatile flow generation ($E = C^{-1}$).

$$E(t) = (E_{max} - E_{min})E_n(t) + E_{min} \tag{2}$$

where $E_n(t)$ is a normalized elastance function which has been used in an adult model (Stergiopulos et al., 1996) that we modified for the fetal model as

$$E_n(t) = 1.67\left[\frac{(t.\mathrm{HR}/0.303)^{1.32}}{1+(t.\mathrm{HR}/0.303)^{1.32}}\right]\left[\frac{1}{1+(t.\mathrm{HR}/0.508)^{21.9}}\right] \tag{3a}$$

for the ventricles

$$E_n(t) = 2.70\left[\frac{(t.\mathrm{HR}/0.303)^{1.32}}{1+(t.\mathrm{HR}/0.303)^{1.32}}\right]\left[\frac{1}{1+(t.\mathrm{HR}/0.25)^{21.9}}\right] \tag{3b}$$

for the atria where HR is the heart rate. The four heart valves and foramen ovale were modeled as unidirectional resistance.

Reference C, R, E_{max} and E_{min} values were adopted from (Pennati et al., 1997) and (Sa-Couto et al., 2010), then calibrated to match blood pressures at the umbilical vein, cardiac output and organ flow distribution of a near-term human fetus (40 weeks, fetal weight = 3500 g) using clinical data (Kiserud et al., 2006; Mielke and Benda, 2001; Molina et al., 2008; Rasanen et al., 1996; Rudolph, 2009; Ville et al., 1994). All LPM parameter values are provided in the Supplementary data.

2.2. Gas exchange model

Gas transport in the cardiovascular system is governed by Eq. (4).

$$\frac{d(V[O_2])_i}{dt} = \sum_{\substack{Q_{ji}>0 \\ j=1}}^{N} Q_{ji}([O_2]_j + [O_2]_{in,ji}) - \sum_{\substack{Q_{ij}>0 \\ j=1}}^{N} Q_{ij}[O_2]_i - \dot{M}_i \tag{4}$$

where $[O_2]_{in,ji}$ is the increase in $[O_2]$ due to oxygen intake over the respiratory element between compartments i and j, and $\dot{M}_i$ is the metabolic consumption rate.

A gas exchange model based on lumped alveolar-capillary gas diffusion mechanics (Hoppensteadt et al., 2002; Kowalski et al., 2010) was adopted for the lungs. $[O_2]_{in,ji}$ of the lungs is governed by the respiratory gas exchange Eq. (5). Subscripts refer to compartment labels in Fig. 1, unless otherwise is stated. For convenience, pulmonary respiration takes place in the pulmonary arterial bed (PAB) in the LPM.

$$[O_2]_{in,PAB} = r[O_2]_I - r\frac{\mathrm{H}([O_2]_{in,PAB} + [O_2]_{PA})}{\gamma_{PAB}KT} + r\frac{(1-\gamma_{PAB})\mathrm{H}([O_2]_{PA})}{\gamma_{PAB}KT} \tag{5}$$

where r is the ratio of ventilation rate to blood perfusion rate averaged over all alveolo-capillary units of the lung, $[O_2]_I$ is the oxygen concentration of inspired air, $[O_2]_{PA}$ is the oxygen concentration of the pulmonary arteries entering the lung, $[O_2]_{in,PAB}$ is the increase in oxygen concentration of the blood flow passing through the pulmonary arterial bed, $\mathrm{H}([O_2])$ is the oxygen–hemoglobin dissociation curve represented by the Hill function and gives the partial pressure of oxygen (PO_2) in fetal blood, K is the ideal gas constant, T is the absolute temperature, and γ_{PAB} is a respiration efficiency parameter ($\gamma \in [0,1]$) that adjusts the level of equilibrium between blood and air PO_2 at the exit of pulmonary capillaries. Blood and alveolar air PO_2 fully equilibrate when $\gamma = 1$ (assumed case for lungs in this model), and there is no oxygen exchange if $\gamma = 0$. Eq. (5) is modified for the placental respiration, producing Eq. (6).

$$[O_2]_{in,PB} = r[O_2]_U - rH_M^{-1}\left(\frac{\mathrm{H}([O_2]_{in,PB} + [O_2]_{PLAC})}{\gamma_{PB}} + \frac{(1-\gamma_{PB})\mathrm{H}([O_2]_{PLAC})}{\gamma_{PB}}\right) \tag{6}$$

where H_M^{-1} is the inverse Hill function representing the maternal oxygen–hemoglobin dissociation curve, $[O_2]_U$ is the oxygen concentration in uterine arteries, $[O_2]_{PLAC}$ is the oxygen concentration of the umbilical arteries entering the placenta, $[O_2]_{in,PB}$ is the increase in oxygen concentration of the blood flow through the placental bed, and γ_{PB} is the placental respiration efficiency. In Eq. (6), r is calculated as the ratio of the fetal placental flow rate to an assumed maternal uterine flow rate of 600 ml/min. A detailed description of the gas exchange models is presented in the Supplementary information.

Organ level metabolic consumption is distributed such as to match oxygen saturation (SO_2) levels obtained from fetal lambs, although metabolic differences between human and lamb were taken into account (Rudolph, 2009). Simulated SO_2 were compared to umbilical cord oxygen measurements in the fetus and newborn (Lackman et al., 2001; Rudolph, 2009). Placental respiration efficiency (γ_{PB}) was calibrated until we achieved an SO_2 of 43.2% at the fetal umbilical arteries and 69.4% at the fetal umbilical vein.

2.3. Fetal transitional shunts

We modeled the transition from the fetal-to-neonatal circuit by prescribing time-varying resistance functions for the closure of umbilical arteries, placental bed, umbilical vein, ductus venosus and ductus arteriosus (UA, PB, iUV, DV, DA respectively); and for the expansion of pulmonary arterial and venous beds (PAB and PVB) (acronyms correspond to transitioning vessels as shown in Fig. 1). We found that transitional dynamic changes in the pulmonary and DA flow (Crossley et al., 2009), pulmonary and aortic pressure (Emmanouilides et al., 1964), and pulmonary flow and pressure (Friedman and Fahey, 1993) were best reflected when relating the DA resistance transition to a linear diameter change assuming Poiseuille resistance law ($R \propto diameter^{-4}$), Eq. (7), and relating the pulmonary vascular resistance (PVR) to a logarithmic decrease in time (Eq. (8)) (Fig. 2a).

$$R_{DA}(t) = \frac{R_0 R_F \tau^4}{\left((t)R_0^{1/4} + (\tau - t)R_F^{1/4}\right)^4} \tag{7}$$

$$\mathrm{PVR}(t) = \frac{R_F}{1 + \left[(R_F/R_0) - 1\right]e^{n((t/\tau))}} \tag{8}$$

where R_0 and R_F are initial (fetal) and final (neonatal) values of resistance (values are provided in Supplementary data), τ defines the amount of time for the resistance to reach its neonatal value, and n is a dimensionless number that determines the shape of the logarithmic function and was adjusted to match an experimentally

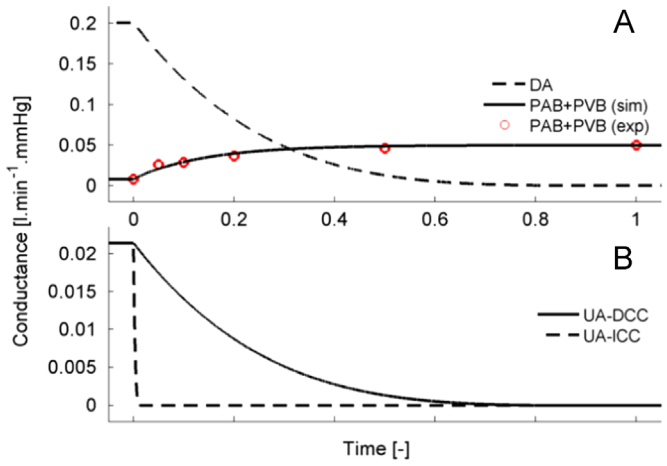

Fig. 2. Vascular conductance changes of selected vessels during the transition period. (A) Conductance history of the ductus arteriosus (DA, *dashed*) and pulmonary vascular bed (PAB+PVB, *solid*) during the transition period. Red markers show the experimentally obtained data points (Crossley et al., 2009), black solid lines represent simulated trend. (B) Umbilical artery (UA) constriction in ICC (*dashed lines*) and DCC (*solid lines*). Complete transition of all vessels was defined to complete at time $=\tau$, and the time axis is normalized to τ. (DCC: delayed cord clamping, ICC: immediate cord clamping).

measured PVR curve of the fetal lamb ($n=-6.931$) (Fig. 2a) (Crossley et al., 2009). τ is specified as 10 min for all transitioning vessels in our model. Foramen ovale resistance was not assigned a transition function but it closed passively under the reversal of pressure gradient between the left and right atria during the course of transition.

In order to model ICC, we set the umbilical vascular resistances to shut immediately at the onset of the transition. In the DCC, umbilical arteries were slowly shut during the 10-min period, while umbilical vein remained open to allow placental transfusion (Fig. 2b) and then clamp was applied at the end of the investigated period. Umbilical arteries (in DCC) and ductus venosus transition were simulated similar to DA as in Eq. (7). Neonatal state resistances of the pulmonary arterial and venous beds were calibrated to match the simulated pulmonary arterial pressure with clinical catheterization measurements made at the same site after birth (Emmanouilides et al., 1964; Kitterman et al., 1969).

Heart rate (140 bpm) and compliances were kept constant through the fetal and neonatal models. The fetus and placenta were assumed to remain at the same height and the effect of gravity was neglected (Vain et al., 2014).

2.4. Transition-gas exchange

The ventilation–perfusion ratio at the lungs increases from zero at the moment of birth to a clinically observed value at 24 h after birth ($r=0.63\pm0.7$) (Koch, 1968), at the end of pulmonary expansion. Owing to the lack of clinical data, we assumed a linear function for the temporal trajectory of r; therefore, findings are of comparative value.

2.5. Numerical method

The resulting system of differential equations is discretized by Backwards Euler scheme (Hoppensteadt et al., 2002; Peskin and Tu, 1986). The implicit scheme is stable regardless of the time step size and the value of resistance parameters (Peskin and Tu, 1986), which allowed us choosing a fixed time step where small and large resistances exist in the LPM. One cardiac cycle was divided in 200 time steps, increasing the number of time steps further did not produce any noticeable improvement in the accuracy of the solution. Nonlinear gas exchange equations are solved through an iterative implementation of the method of bisection (Hoppensteadt et al., 2002). After rearranging Eqs. (5) and (6) by moving the left hand side to the right hand side, the solution to $[O_2]_{in}$ (root of the residual function) was searched using the bisection method within an interval of solutions bounded by a physiological maximum and minimum value for $[O_2]_{in}$. In the trial cases, there was always a single root for the nonlinear residual equation within the range of physiological solutions; therefore, the bisection method was guaranteed to converge. A typical pulsatile simulation of the fetal LPM is provided in the Supplementary Movie 1.

3. Results

3.1. Validation of the fetal-to-neonatal transition: flow and pressures

To ensure the validity of our model, simulated (i) combined cardiac output (CCO) and organ flow distribution, (ii) arterial blood pressures, (iii) flow time tracings, and (iv) dynamic flow-pressure patterns were compared with clinical measurements obtained from healthy term infants before and after birth.

Reference values for CCO and organ-level flow distribution for the fetus were obtained from respective publications (Kiserud et al., 2006; Mielke and Benda, 2001; Molina et al., 2008; Rasanen et al., 1996; Rudolph, 2009), and selected values for organ flow distributions are displayed in Fig. 1 for direct comparison. Simulated fetal CCO was 1510 ml/min, which is in accordance with the reported CCO for term-fetus. The largest disparity in flow distribution between the model and measurements was 28% in hepatic vein, followed by ductus venosus (27%) and inferior vena cava (24%), which are in the standard subject-to-subject deviation. Simulated flow tracings at the atrioventricular valves and the fetal shunts were in good comparison with fetal Doppler velocity waveforms (Hecher et al., 1994; Hiraishi et al., 1987; Huhta et al., 1987; Reed et al., 1986; Wilson et al., 1987) (flow time tracings are presented in Supplementary Movie 1). Simulated mitral and tricuspid *E*/*A* ratios were 0.81 and 0.71, respectively, in the circulation before birth.

Due to the scarcity of *in utero* pressure measurements, validation of arterial pressures was restricted to the neonatal stage. In the simulation of the ICC case, neonatal systolic/diastolic (mean) pressures sampled at the ascending aorta were 64/42 (52) mmHg compared to 71/49 (59) mmHg *in vivo*, whereas the main pulmonary artery pressures were 37/14 (25) mmHg compared to 40/12 (25) mmHg *in vivo*. Results from the simulation agreed with pressure measurements obtained *in vivo* at 10th to 48th hour of life (Emmanouilides et al., 1964; Kitterman et al., 1969). Prenatal fetal umbilical vein pressure in the model (8 mmHg) agreed with clinical measurements (6 mmHg) (Ville et al., 1994).

3.2. Dynamic flow patterns during the transition in immediate and delayed cord clamping

3.2.1. Umbilical cord flow and placental transfusion

In ICC, placental flow was suddenly ceased and no placental transfusion was observed. In DCC, placental volume shift was driven by the positive pressure gradient from the placental bed towards the inferior vena cava ($\Delta P_{PLAC-IVC}=21$ mmHg at $t=0$). Umbilical vein flow rate decreased as the umbilical arteries constricted. A quasi-linear volume shift from the placenta to the neonatal body was observed, 90% of transfusion was achieved midway through the fetal-to-neonatal transition, and there was

practically no further increase in the fetal blood volume during the last 20% of the transition period. In DCC, the placental transfusion volume amounted to 31.3 ml, which increased neonatal blood volume by 11.7%.

3.2.2. Central flow patterns and arterial pressures

Central flow patterns are plotted in Fig. 3. Fig. 3a shows that the DA maintained a cycle-averaged right-to-left flow direction during the early stages of the transition, though it became a bidirectional shunt immediately after. Reversal of the flow is attributed to the reversed pressure gradient across DA, which resulted from the decrease in pulmonary vascular resistance and a simultaneous increase in systemic vascular resistance. The cycle-averaged DA flow direction was reversed to left-to-right earlier in the ICC (at $t=0.07\tau$) compared to DCC (at $t=0.12\tau$).

With the expansion of lungs, pulmonary blood flow rapidly increased to 400% of its baseline fetal value and peaked at 0.3τ in the ICC case and at 0.38τ in the DCC case (Fig. 3b). The apparent relationship between the dynamic pulmonary and DA flow patterns (Fig. 3a and b) indicates that reverse DA flow is the major contributor to the pulmonary flow rate overshoot during mid-transition. Simulated pulmonary and DA flow rates show realistic transition patterns similar to those reported in animal experiments by (Crossley et al., 2009). Foramen ovale closed rapidly under the reversed pressure gradient between the left and right atrium around 0.1τ for both cord clamping cases.

Ventricular outputs are plotted in Fig. 4 (and in Supplementary Movie 2). Shortly after the initial establishment of pulmonary circulation, left ventricular (LV) filling was enhanced with a greater pulmonary venous return that was mainly attributed to the reverse DA flow. Consequently, left ventricle output (LVO) increased two-fold (1430 ml/min in DCC, 1310 ml/min in ICC) and exceeded RVO during the mid-transition. Capturing the previous descriptions of the changes in LVO in human newborns (Agata et al., 1991), closure of DA was largely responsible for the gradual decrease in pulmonary blood flow and LVO during the latter half of the transition. At the end of the transition, the systemic and pulmonary circulations are separated and LVO and RVO equilibrated to 993 ml/min in ICC and 1197 ml/min in DCC. Besides differences in their magnitudes, transitional trends were similar for ventricular outputs in DCC and ICC.

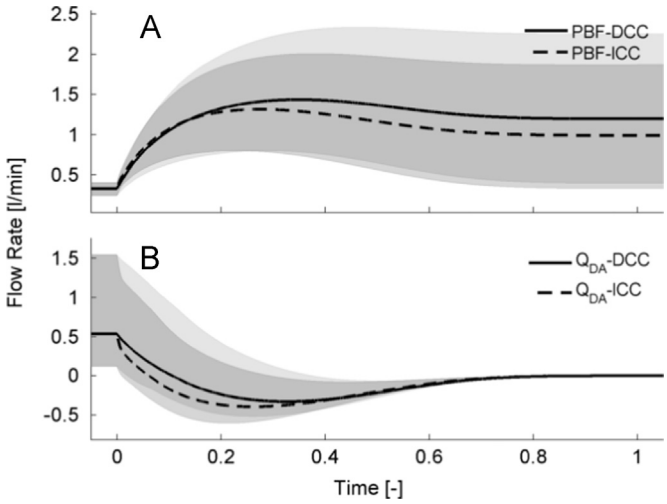

Fig. 3. Effects on pulmonary perfusion. Comparison of the ductus arteriosus blood flow (Q_{DA}) and the pulmonary blood flow (PBF), during the transition. (A) Cardiac-cycle averaged Q_{DA}, positive values indicate a right-to-left shunt. Predominant flow reversal occurs earlier in ICC compared to DCC (at time$=0.07\tau$ *vs.* 0.12τ). For the rest of the transition, DA is primarily a left-to-right shunt. (B) Cardiac-cycle averaged PBF increases rapidly with expanding lungs. DA reverse flow is the major contributor to the pulmonary flow shift during mid-transition. *Solid* and *dashed* curves represent DCC and ICC cases, respectively. Shaded areas represent the maximum and minimum pulsatile flow during a cardiac cycle, dark gray: ICC, light gray: DCC. Complete transition of all vessels was defined to complete at time$=\tau$, and the time axis is normalized to τ. (DCC: delayed cord clamping, ICC: immediate cord clamping).

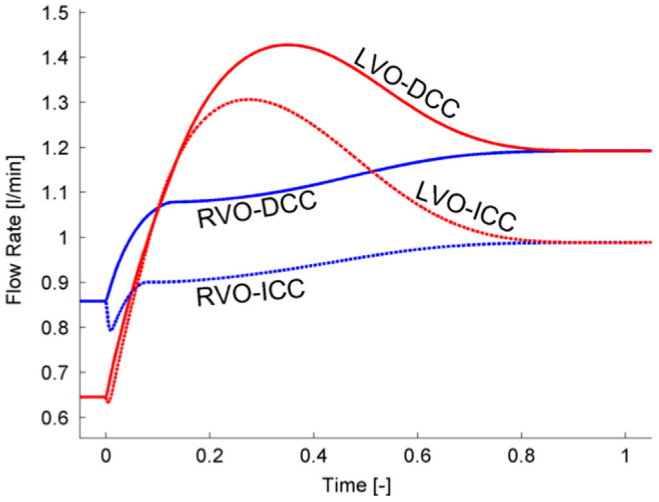

Fig. 4. Mean ventricular function during fetal transition for DCC and ICC. Cardiac-cycle averaged left (*red*) and right (*blue*) ventricular outputs (LVO and RVO) during the transition. *Solid* and *dashed* lines represent DCC and ICC cases, respectively. Complete transition of all vessels was defined to complete at time$=\tau$, and the time axis is normalized to τ. (DCC: delayed cord clamping, ICC: immediate cord clamping).

Dynamic changes in arterial blood pressures are plotted in Fig. 5 (and in Supplementary Movie 2). At the beginning of the transition, a pressure wave in the systemic and pulmonary arteries (with a magnitude of 2.8 mmHg at the main pulmonary artery and 3.7 mmHg at the ascending aorta) was observed in the ICC case due to the sudden increase in systemic resistance associated with clamping. Overall, DCC favored higher arterial blood pressures compared to ICC by 20%, with 77/50 (63) mmHg at the ascending aorta, and 44/17 (30) mmHg at the main pulmonary artery in DCC.

3.2.3. Ventricular pressure–volume curves

Ventricular pressure–volume curves are presented in Fig. 6. In both clamping scenarios, afterload increased for the LV, and decreased for the right ventricle (RV). In DCC, the end-diastolic volume of the RV increased from 10.4 ml to 11.7 ml, whereas in the ICC it reduced to 9.9 ml. Increase in RV stroke volume was mainly attributed to an increased ejection fraction (EF_{RV}, fetal: 60% neonate: 73%). In the LV, the increase in end-diastolic volume (fetal: 6.5 ml, DCC: 12.1 ml, ICC: 9.6 ml) and slight increase in ejection fraction (EF_{LV}, fetal: 70% neonate: 74%) contributed to the increase in stroke volume.

Since the heart rate was kept constant throughout the simulation, this increase in cardiac output with DCC (approximately by 20% compared to ICC) is solely attributed to an increased preload (by 21%) which induced a higher stroke volume through the Frank–Starling mechanism, which is clearly visible in the pressure–volume curves of ventricles (Fig. 6).

3.3. Gas exchange and oxygen saturation during fetal transition

Fig. 7 summarizes the impact of cord clamping on the SO_2 in the systemic aorta and the carotid arteries. Under the simulated conditions, ICC SO_2 levels were significantly lower than DCC, and encountered a 15–20% decrement in arterial SO_2 during the early

transition. At $t=0.1\tau$, DCC and ICC carotid SO_2 were 51.3% and 26.3%, respectively. For DCC, 90% SO_2 was reached at 0.27τ through the transition, in the ICC case, an additional 0.1τ was needed to reach 90% SO_2. Simulated SO_2 values were in good agreement with clinical reference ranges for ICC (Dawson et al., 2010) and for DCC (Smit et al., 2014).

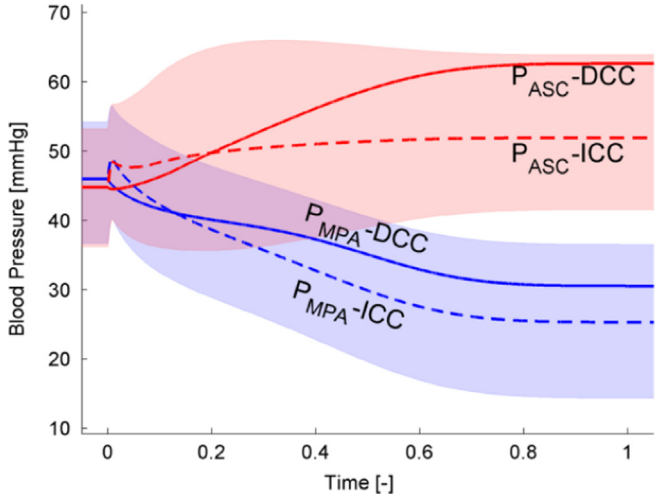

Fig. 5. Mean arterial pressure changes during the transition for DCC (*solid* lines) *vs.* ICC (*dashed* lines) in the ascending aorta (ASC, *red*) and main pulmonary artery (MPA, *blue*). DCC blood pressures were higher during most of the transition period and remained greater than ICC pressures even at the end of the transition. ICC generated a pressure wave (which had a magnitude of 2.8 mmHg at the MPA, and 3.7 mmHg at the ASC) during the early transition period. Shaded areas plotted only for ICC represent the maximum and minimum pulsatile pressures during a cardiac cycle, red shade: P_{ASC}, blue shade: P_{MPA}. Complete transition of all vessels was defined to complete at time$=\tau$, and the time axis is normalized to τ. (P: pressure, DCC: delayed cord clamping, ICC: immediate cord clamping). (For interpretation of the references to color in this figure, the reader is referred to the web version of this article.)

4. Discussion

4.1. Placental transfusion improves ventricular function and hemodynamic stability

An important component of our model, which was not resolved by the previous animal or human studies (Bhatt et al., 2013; Sommers et al., 2012) is the role of placental transfusion in DCC. Following birth umbilical vein stays open and umbilical arteries constrict with increasing oxygen saturation, which allows the placental blood to flow towards the infant's circulation as demonstrated in the clinic (McGrath et al., 1986; Mercer and Skovgaard,

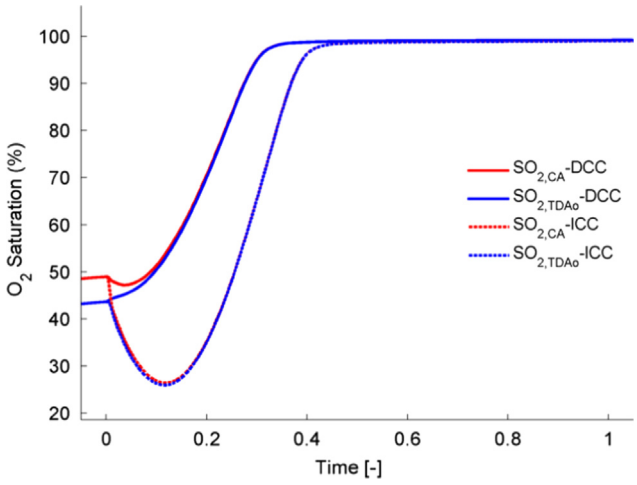

Fig. 7. Oxygen saturation trends were different for DCC and ICC circulations. In ICC, a drop in the oxygen levels was observed before the lung ventilation stabilized. Depending on the duration of fetal transition this can be significant. Oxygen saturations were sampled at the carotid arteries ($SO_{2,CA}$) and at the thoracic descending aorta ($SO_{2,TDAo}$). Complete transition of all vessels was defined to complete at time$=\tau$, and the time axis is normalized to τ. (DCC: delayed cord clamping, ICC: immediate cord clamping).

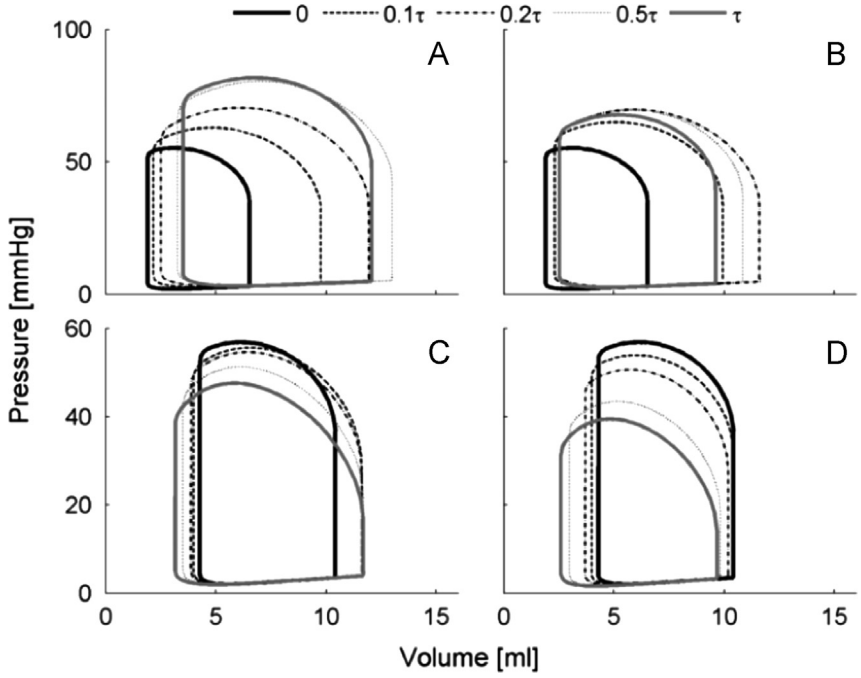

Fig. 6. Pressure–volume (PV) loops sampled for one cardiac cycle at different time points during the transition. The legend at the top shows the time point for each sample. (A) PV curve for the LV in DCC. (B) PV curve for the LV in ICC. (C) PV curve for the RV in DCC. (D) PV curve for the RV in ICC. Complete transition of all vessels was defined to complete at time$=\tau$, and the time axis is normalized to τ. (LV: left ventricle, RV: right ventricle, DCC: delayed cord clamping, ICC: immediate cord clamping).

2002). If both vessels constrict at the same time, the placental blood is trapped inside the placenta. In our DCC simulation, the infant's blood volume is increased by 11.7%, which resulted with a *persistent* increase in the preload (venous pressure) by 20% in relation with the whole-body vascular compliance (3.6 ml/mmHg kg^{-1}) (Brace and Gold, 1984). Reported transfusion volume for 5 min DCC was 166 ml (60% increase in blood volume) (Usher et al., 1963). Following to the transfusion, it was observed that blood volume decreased rapidly due to plasma transudation and the net increase in blood volume from birth to four hours in life was 14.1%. This value is in good agreement with our model results implying that simulated conditions are compatible with the early transition phase of the neonate.

The relation between afterload, preload, and ventricular stiffness/contractility resulted in an increase in stroke volume by 21% in DCC compared to ICC. This finding is supported by *in vivo* observations where CO and superior vena cava flow was greater in DCC groups (Bhatt et al., 2013; Sommers et al., 2012). The relation between stroke volume and preload can depend on the ventricular model that is used. In our trial simulations (results not shown here) using a variable volume intercept elastance model (Lankhaar et al., 2009) stroke volume increase was 20% with a transfusion of 53 ml (corresponding preload increase was 50%). We should remark that the *in vivo* impact of placental transfusion on the CO can also be influenced by autoregulation and baroreflex effects such as changes in peripheral resistance, venous tone, myocardial contractility, heart rate, and homeostatic mechanisms that may act to conserve the blood volume level, including transudation.

4.2. Delayed cord clamping improves oxygenation at birth

We observed that DCC can significantly improve the oxygen saturation during the early transitional period when lungs are not yet fully active (Fig. 7). In our findings, it is clear that placental respiration helps conserving arterial oxygen levels in case pulmonary respiration falls short. This finding indicates that for clinical cases that require newborn resuscitation, it could be the best practice to preserve the placental circulation in order to prevent severe hypoxia/asphyxia unless failure of placental function is the cause for the need of resuscitation (Niermeyer and Velaphi, 2013).

The initial brief drop in arterial oxygen concentrations computed for ICC case in our simulations (arterial SO_2, fetal: 45% ICC 1st min: 27%) were not reported during the clinical measurements. A possible explanation can be attributed to the pulse oximetry techniques (Dawson et al., 2010; Saugstad, 2006) that can only be applied after the first minute in life. It is clearly observed from our model that DCC significantly helps the oxygenation of the newborn circulation. The clinical standard recommends that the peripheral SO_2 should reach 90% during the first 10 min (median 7.9 min (Dawson et al., 2010)). However, this standard is established mainly based on newborns who underwent ICC (Dawson et al., 2010; Saugstad, 2006). With DCC, it is possible to increase the rate of oxygenation as recent clinical trials showed that peripheral SO_2 in DCC is higher than ICC immediately after birth (Smit et al., 2014). Our oxygen model calculations predicted that postnatal oxygen saturations to reach 90% requires less time with DCC than ICC.

4.3. Predictive capabilities and accuracy of the present model

The time-varying resistance transition model employed in our simulations captured the essential cardiovascular events observed *in vivo* during and after birth that can be seen in the simulated dynamics in DA and pulmonary flow rates (Fig. 3), ventricular outputs (Fig. 4), arterial pressures (Fig. 5), the effects of cord clamping on the hemodynamics and gas levels (Figs. 3–7) and the changes in atrioventricular *E*/*A* ratios (Table 2). A summary of the predictive capabilities of our model is summarized in Table 2.

4.4. Ductus arteriosus flow patterns and indications on shunt remodeling

In ICC, the instantaneous removal of the placental circulation caused systemic pressure to increase rapidly and surpass the pulmonary pressure in less time compared to DCC. This led to an earlier reversal of the flow across the DA (Fig. 3a). Oxygen concentration through the DA in relation to the timing and the magnitude of the shunt flow can alter the remodeling of the DA diameter. For precise timing, computed oxygen concentration can be linked to the DA constriction (Heymann and Rudolph, 1975; Nakanishi et al., 1993; Oberhansli-Weiss et al., 1972) where an

Table 2
Summary of the major hemodynamic events in the fetal to neonatal transition observed in the clinical practice and assessment of our model on its ability to capture them in its predictions.

Dynamic changes in cardiovascular function at birth	Prediction	Comparison criteria	Reported	Simulated
Central flow patterns (DA, pulmonary) (Crossley et al., 2009)[a]	Captured	Change in DA and PBF	DA: −227% PBF: +1200% at 10 min	DA: −200% PBF: +400% at $t\sim 0{,}2\tau$
Temporal increase in LVO after birth (Agata et al., 1994)	Captured	Change in LVO from fetal to neonatal	200% at 1 h	200% at $t\sim 0.27\tau$
Systemic and pulmonary blood pressure separation (Emmanouilides et al., 1964; Kitterman et al., 1969)	Captured	Systemic-pulmonary pressure gradient	~35 mmHg at 96 h	~30 mmHg at $t=\tau$
Change in the *E*/*A* ratios of atrioventricular flow time tracings (Wilson et al., 1987)	Captured	Tricuspid and Mitral E/A ratios (fetal→newborn)	Tri:0.8→0.8 Mit:0.8→1.17	Tri:0.76→0.87 Mit:0.81→1.05 at $t=\tau$
Placental transfusion with DCC (Usher et al., 1963)	Captured	Increase in blood volume	14.1% at 4 h	11.7% at $t=\tau$
Long-term improvement of RVO and SVC flow with DCC (Sommers et al., 2012)	Captured	Increase in SVC flow	20% between 6 h and 96 h	20% at $t=\tau$
Decreased CO immediately after birth with ICC (Bhatt et al., 2013)[a]	Captured	Decrease in RVO	65% at 0–90 s	11% at $t=0$
Increased afterload immediately after birth with ICC (Bhatt et al., 2013)[a]	Captured	Increase in arterial BP	34% at 0–30 s	9% at $t=0$
Bradycardia in ICC (Bhatt et al., 2013)[a]	Not captured	Reduction in heart rate	40% at 120 s	Not modeled
Higher SpO_2 in the early transition with DCC (Smit et al., 2014)	Captured	Difference in SO_2 in DCC compared to ICC	11% higher at 1 min	25% higher at $t=0.1\tau$

[a] Reported measurements are obtained from fetal lamb experiments. In Bhatt et al.'s study lambs were not ventilated for 120 s after cord clamping. DA: ductus arteriosus, PBF: pulmonary blood flow, LVO: left ventricular output, RVO: right ventricular output, SpO_2: peripheral oxygen saturation, DCC: delayed cord clamping, ICC: immediate cord clamping.

earlier influx of oxygen rich blood from the left heart may cause premature reduction of the DA diameter. Further, placental transfusion can help preventing premature constriction of DA since placental blood contains prostaglandins, which are vasodilators of the DA. However, it is unknown to which extent the prostaglandins in the placental circulation play a role in the transition with placental transfusion.

The presence of a continued placental oxygen supply at birth can play a major role in the expansion of pulmonary circulation due to the vasoactive properties of oxygen. After the closure of foramen ovale (that occurs in a short time after birth), all the placental return is directed to the RV and lungs. As a result, the lung vessels will receive a greater portion of the oxygenated placental blood, which should lead to further vasodilatation or at least preventing vasoconstriction, which might occur with deoxygenated blood.

4.5. Effect of transition time

All transition times in the model were set to 10 min, which is considered typical for pulmonary circulation, but can be short for the ductal transition which normally takes place in 2 days. Therefore, we also tested several different transition times for DA, pulmonary, and the placental circulation, and the effects of their relative shifts. This additional verification study showed that the predicted transitional trends were similar in all simulations (data not shown for brevity). However, there were slight changes in the timing of hemodynamic events. DA reversal occurred earlier with a faster constriction of umbilical arteries in DCC. If the DA constriction was slowed, temporal overshoot in pulmonary flow rate and LVO during the patent DA became more significant.

4.6. The effect of pulmonary vascular expansion

In fetus, lungs are found in a hyperinflated state due to the high volume of lung fluid filling the airspaces in the alveoli. At birth following the replacement of lung fluid with air, PVR rapidly decreases due to the volume expansion of pulmonary capillaries under increased transmural pressure gradient and vasodilatory effects (Gao and Raj, 2010). Capillary expansion requires the vascular walls to undergo large radial deformations. Under normal conditions, pulmonary pressure–volume relation is linear and the slope is determined by the constant pulmonary compliance (Fung, 1997), therefore it may be expected that pulmonary compliance to not change with the radial expansion of capillaries. However, during transition several factors that affect the compliance may come into play such as an increase in number of active capillaries contributing to the organ vascular compliance, changes in structural stiffness due to lung volume variations and strain-dependent elasticity of the lung parenchymal tissue, mechanical instabilities, vasodilation, changes in surface tension at the air–liquid interface, and short term vascular remodeling that follows the expansion (Elad et al., 1988; Fung, 1997; Gao and Raj, 2010; Gefen et al., 1999). Therefore, in order to observe the effect of a potential increase in pulmonary vascular compliance we simulated an additional case in which pulmonary capillary compliance (lung compartment in Fig. 1) was varied proportional to $R^{-3/4}$ considering that $R \propto diameter^{-4}$ and $C \propto diameter^{3}$. Blood volume in pulmonary capillaries increased with the subsequent increase in capillary compliance resulting in a decrease in blood volumes in other organ compartments. Consequently, we observed a decrease in neonatal cardiac output and arterial blood pressures by 10% from the values reported in Section 3, but transitional hemodynamic trends and the relative difference between ICC and DCC did not change. This additional sensitivity study highlights the role of DCC in maintaining cardiac output and organ blood volume levels when pulmonary circulation is expanding.

4.7. Limitations

Although our model has been rigorously compared to the clinically measured data and agrees well with qualitative clinical studies and clinical expertise, the inherent limitations of this work are acknowledged. The biochemical responses at birth, detailed lung expansion and liquid clearance, metabolic adjustments, cardiopulmonary interactions, homeostatic control, autoregulation and baroreflex response, as well as detailed systemic compartments have not been modeled, in order to achieve a simpler model with fewer variables.

5. Conclusion

Quantitative knowledge of gestational hemodynamics is crucial in the management of neonatal care. We constructed a system-level LPM of the fetal-to-neonatal transition in human, which is validated with the existing *in vivo* clinical data. This model demonstrates that ICC can lead to an earlier onset of DA flow reversal and a reduced CO. Meanwhile, DCC imposes increased blood pressures due to an increased blood volume, and a higher CO through the Frank–Starling mechanism. For cases where the pulmonary ventilation is gradually established or delayed, ICC caused critically low arterial oxygen saturations due to rapidly depleting oxygen stores, whereas DCC prevented the oxygen levels to drop below the critical threshold by continued placental respiration. Our findings contribute to the literature by demonstrating the link between placental transfusion in DCC and increased cardiorespiratory performance in the term infant.

Conflict of interest statement

None.

Further statement

Our submitted study and manuscript are achieved through the substantial contributions of all authors to all of the following:

(1) the conception and design of the study, or acquisition of data, or analysis and interpretation of data;
(2) drafting the article or revising it critically for important intellectual content;
(3) final approval of the version to be submitted.

Likewise our manuscript, including related data, figures and tables has not been previously published and that the manuscript is not under consideration elsewhere.

Acknowledgments

This study is supported through funding provided by NSF 0954465, EU-FP7 307460 and TUBITAK 2215.

Appendix A. Supporting information

Supplementary data associated with this article can be found in the online version at http://dx.doi.org/10.1016/j.jbiomech.2015.02.040.

References

Agata, Y., Hiraishi, S., Misawa, H., Hirota, H., Nowatari, M., Hiura, K., Fujino, N., Oguchi, K., Horiguchi, Y., 1994. Regional blood flow distribution and left ventricular output during early neonatal life: a quantitative ultrasonographic assessment. Pediatr. Res. 36, 805–810.

Agata, Y., Hiraishi, S., Oguchi, K., Misawa, H., Horiguchi, Y., Fujino, N., Yashiro, K., Shimada, N., 1991. Changes in left ventricular output from fetal to early neonatal life. J. Pediatr. 119, 441–445.

Bhatt, S., Alison, B.J., Wallace, E.M., Crossley, K.J., Gill, A.W., Kluckow, M., te Pas, A.B., Morley, C.J., Polglase, G.R., Hooper, S.B., 2013. Delaying cord clamping until ventilation onset improves cardiovascular function at birth in preterm lambs. J. Physiol. 591, 2113–2126.

Boere, I., Roest, A., Wallace, E., ten Harkel, A., Haak, M., Morley, C., Hooper, S., Te Pas, A., 2015. Umbilical blood flow patterns directly after birth before delayed cord clamping. Arch. Dis. Child.-Fetal Neonatal Ed. 100, F121–F125.

Brace, R.A., Gold, P.S., 1984. Fetal whole-body interstitial compliance, vascular compliance, and capillary filtration coefficient. Am. J. Physiol. 247, R800–R805.

Coceani, F., Olley, P.M., 1973. The response of the ductus arteriosus to prostaglandins. Can. J. Physiol. Pharmacol. 51, 220–225.

ACOG's Committee on Obstetric Practice, 2012. Committee opinion no.543: timing of umbilical cord clamping after birth. Obstet. Gynecol. 120, 1522–1526.

Crossley, K.J., Allison, B.J., Polglase, G.R., Morley, C.J., Davis, P.G., Hooper, S.B., 2009. Dynamic changes in the direction of blood flow through the ductus arteriosus at birth. J. Physiol. 587, 4695–4704.

Dawson, J.A., Kamlin, C.O., Vento, M., Wong, C., Cole, T.J., Donath, S.M., Davis, P.G., Morley, C.J., 2010. Defining the reference range for oxygen saturation for infants after birth. Pediatrics 125, e1340–e1347.

Elad, D., Kamm, R.D., Shapiro, A.H., 1988. Tube law for the intrapulmonary airway. J. Appl. Physiol. 65, 7–13.

Emmanouilides, G.C., Moss, A.J., Duffie Jr., E.R., Adams, F.H., 1964. Pulmonary arterial pressure changes in human newborn infants from birth to 3 days of age. J. Pediatr. 65, 327–333.

Friedman, A.H., Fahey, J.T., 1993. The transition from fetal to neonatal circulation: normal responses and implications for infants with heart disease. Semin. Perinatol. 17, 106–121.

Fung, Y.-C., 1997. Biomechanics: Circulation. Springer-Verlag, New York.

Gao, Y., Raj, J.U., 2010. Regulation of the pulmonary circulation in the fetus and newborn. Physiol. Rev. 90, 1291–1335.

Gefen, A., Elad, D., Shiner, R., 1999. Analysis of stress distribution in the alveolar septa of normal and simulated emphysematic lungs. J. Biomech. 32, 891–897.

Hecher, K., Campbell, S., Snijders, R., Nicolaides, K., 1994. Reference ranges for fetal venous and atrioventricular blood flow parameters. Ultrasound Obstet. Gynecol. 4, 381–390.

Heymann, M.A., Rudolph, A.M., 1975. Control of the ductus arteriosus. Physiol. Rev. 55, 62–78.

Hiraishi, S., Horiguchi, Y., Misawa, H., Oguchi, K., Kadoi, N., Fujino, N., Yashiro, K., 1987. Noninvasive Doppler echocardiographic evaluation of shunt flow dynamics of the ductus arteriosus. Circulation 75, 1146–1153.

Hoppensteadt, F.C., Peskin, C.S., Hoppensteadt, F.C., 2002. Modeling and Simulation in Medicine and the Life Sciences, 2nd ed. Springer, New York.

Huhta, J.C., Moise, K.J., Fisher, D.J., Sharif, D.S., Wasserstrum, N., Martin, C., 1987. Detection and quantitation of constriction of the fetal ductus arteriosus by Doppler echocardiography. Circulation 75, 406–412.

Huikeshoven, F.J., Hope, I.D., Power, G.G., Gilbert, R.D., Longo, L.D., 1985. Mathematical model of fetal circulation and oxygen delivery. Am. J. Physiol. 249, R192–R202.

Hutchon, D.J., 2013. Early vs delayed cord clamping at birth; in sickness and in health. Fetal Matern. Med. Rev.

Kiserud, T., Ebbing, C., Kessler, J., Rasmussen, S., 2006. Fetal cardiac output, distribution to the placenta and impact of placental compromise. Ultrasound Obstet. Gynecol. 28, 126–136.

Kitterman, J.A., Phibbs, R.H., Tooley, W.H., 1969. Aortic blood pressure in normal newborn infants during the first 12 h of life. Pediatrics 44, 959–968.

Koch, G., 1968. Alveolar ventilation, diffusing capacity and the A-a PO_2 difference in the newborn infant. Respir. Physiol. 4, 168–192.

Kowalski, W., Dur, O., Pekkan, K., 2010. Lumped parameter model for the measurement of o_2 and co_2 concentration in congenital heart defects. In: Proceedings of the BMES Annual Fall Meeting. Austin, TX.

Lackman, F., Capewell, V., Gagnon, R., Richardson, B., 2001. Fetal umbilical cord oxygen values and birth to placental weight ratio in relation to size at birth. Am. J. Obstet. Gynecol. 185, 674–682.

Lankhaar, J.W., Rovekamp, F.A., Steendijk, P., Faes, T.J., Westerhof, B.E., Kind, T., Vonk-Noordegraaf, N., Westerhof, N., 2009. Modeling the instantaneous pressure–volume relation of the left ventricle: a comparison of six models. Ann. Biomed. Eng. 37, 1710–1726.

McGrath, J.C., MacLennan, S.J., Mann, A.C., Stuart-Smith, K., Whittle, M.J., 1986. Contraction of human umbilical artery, but not vein, by oxygen. J. Physiol. 380, 513–519.

Mercer, J.S., Skovgaard, R.L., 2002. Neonatal transitional physiology: a new paradigm. J. Perinat. Neonatal Nursing 15, 56–75.

Mielke, G., Benda, N., 2001. Cardiac output and central distribution of blood flow in the human fetus. Circulation 103, 1662–1668.

Molina, F.S., Faro, C., Sotiriadis, A., Dagklis, T., Nicolaides, K.H., 2008. Heart stroke volume and cardiac output by four-dimensional ultrasound in normal fetuses. Ultrasound Obstet. Gynecol. 32, 181–187.

Nakanishi, T., Gu, H., Hagiwara, N., Momma, K., 1993. Mechanisms of oxygen-induced contraction of ductus arteriosus isolated from the fetal rabbit. Circ. Res. 72, 1218–1228.

Niermeyer, S., Velaphi, S., 2013. Promoting physiologic transition at birth: re-examining resuscitation and the timing of cord clamping. Semin. Fetal Neonatal Med. 18, 385–392.

Oberhansli-Weiss, I., Heymann, M.A., Rudolph, A.M., Melmon, K.L., 1972. The pattern and mechanisms of response to oxygen by the ductus arteriosus and umbilical artery. Pediatr. Res. 6, 693–700.

Pekkan, K., Frakes, D., De Zelicourt, D., Lucas, C.W., Parks, W.J., Yoganathan, A.P., 2005. Coupling pediatric ventricle assist devices to the Fontan circulation: simulations with a lumped-parameter model. ASAIO J. 51, 618–628.

Pennati, G., Bellotti, M., Fumero, R., 1997. Mathematical modelling of the human foetal cardiovascular system based on Doppler ultrasound data. Med. Eng. Phys. 19, 327–335.

Pennati, G., Fumero, R., 2000. Scaling approach to study the changes through the gestation of human fetal cardiac and circulatory behaviors. Ann. Biomed. Eng. 28, 442–452.

Peskin, C.S., Tu, C., 1986. Hemodynamics in congenital heart disease. Comput. Biol. Med. 16, 331–359.

Raju, T.N., 2013. Timing of umbilical cord clamping after birth for optimizing placental transfusion. Curr. Opin. Pediatr. 25, 180–187.

Rasanen, J., Wood, D.C., Weiner, S., Ludomirski, A., Huhta, J.C., 1996. Role of the pulmonary circulation in the distribution of human fetal cardiac output during the second half of pregnancy. Circulation 94, 1068–1073.

Reed, K.L., Meijboom, E.J., Sahn, D.J., Scagnelli, S.A., Valdes-Cruz, L.M., Shenker, L., 1986. Cardiac Doppler flow velocities in human fetuses. Circulation 73, 41–46.

Rudolph, A.M., 1970. The changes in the circulation after birth. Their importance in congenital heart disease. Circulation 41, 343–359.

Rudolph, A.M., 2009. Congenital Diseases of the Heart: Clinical-Physiological Considerations, 3rd ed. Wiley-Blackwell, Chichester, UK; Hoboken, NJ.

Sa-Couto, C.D., Andriessen, P., Van Meurs, W.L., Ayres-de-Campos, D., Sa-Couto, P.M., 2010. A model for educational simulation of hemodynamic transitions at birth. Pediatr. Res. 67, 158–165.

Saugstad, O.D., 2006. Oxygen saturations immediately after birth. J. Pediatr. 148, 569–570.

Smit, M., Dawson, J.A., Ganzeboom, A., Hooper, S.B., van Roosmalen, J., Te Pas, A.B., 2014. Pulse oximetry in newborns with delayed cord clamping and immediate skin-to-skin contact. Archives of disease in childhood. Fetal Neonatal Ed.

Sommers, R., Stonestreet, B.S., Oh, W., Laptook, A., Yanowitz, T.D., Raker, C., Mercer, J., 2012. Hemodynamic effects of delayed cord clamping in premature infants. Pediatrics 129, e667–e672.

Stergiopulos, N., Meister, J.J., Westerhof, N., 1996. Determinants of stroke volume and systolic and diastolic aortic pressure. Am. J. Physiol. 270, H2050–H2059.

Suga, H., Sagawa, K., Shoukas, A.A., 1973. Load independence of the instantaneous pressure–volume ratio of the canine left ventricle and effects of epinephrine and heart rate on the ratio. Circ. Res. 32, 314–322.

Sundareswaran, K.S., Pekkan, K., Dasi, L.P., Whitehead, K., Sharma, S., Kanter, K.R., Fogel, M.A., Yoganathan, A.P., 2008. The total cavopulmonary connection resistance: a significant impact on single ventricle hemodynamics at rest and exercise. Am. J. Physiol. Heart Circ. Physiol. 295, H2427–H2435.

Usher, R., Shephard, M., Lind, J., 1963. The blood volume of the newborn infant and placental transfusion. Acta Paediatr. 52, 497–512.

Vain, N.E., Satragno, D.S., Gorenstein, A.N., Gordillo, J.E., Berazategui, J.P., Alda, M.G., Prudent, L.M., 2014. Effect of gravity on volume of placental transfusion: a multicentre, randomised, non-inferiority trial. Lancet 384, 235–240.

Ville, Y., Sideris, I., Hecher, K., Snijders, R.J., Nicolaides, K.H., 1994. Umbilical venous pressure in normal, growth-retarded, and anemic fetuses. Am. J. Obstet. Gynecol. 170, 487–494.

Wilson, N., Reed, K., Allen, H.D., Marx, G.R., Goldberg, S.J., 1987. Doppler echocardiographic observations of pulmonary and transvalvular velocity changes after birth and during the early neonatal period. Am Heart J. 113, 750–758.